charging accumulated in the wires. This observation suggests that the electrical conductivity of the implanted wires was much improved compared to the non-implanted SiNWs.

The formation mechanism of $NiSi_2$ and $CoSi_2$ is schematically shown in Figure 4. At room temperature, the as-grown SiNWs were implanted with Ni^+ or Co^+ ions to a relatively high dose (Fig. 4a). Since the incident ion beam is directional, only the side of the sample facing the ion beam was im-
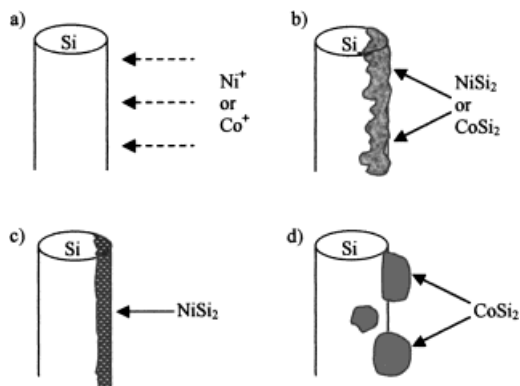

Fig. 4. The formation mechanism of $NiSi_2$/Si and $CoSi_2$/Si on the surface of bare SiNWs. a) Bare SiNWs implanted with metal ions. b) Formation of the metal/Si mixture layer on one side of SiNW. c) The $NiSi_2$/Si nanowire after low temperature annealing. d) $CoSi_2$ nanoparticles formed by coarsening at high temperature annealing.

planted. The SiO_x layer of SiNWs was no longer detected after the implantation, which suggested that the SiO_x layer of SiNWs was probably removed by metal ion implantation. The implanted ions combined with the Si crystalline core to form a mixture of metal/Si (or clusters). The energy of the ion beam is critical since too high an ion energy would result in excessive damage of the SiNWs. We found that 5 kV ions were optimal for the formation of MS/SiNWs. The metal/Si layers contained a high density of defects, or phase damage after the ion implantation. To reduce the defects in the metal/Si layer, the as-implanted wires were annealed. At an annealing temperature of 500–600 °C, the quality of Ni/Si layers can be improved. This is depicted in Figure 4c showing that Ni/Si clusters re-crystallize and form a $NiSi_2$ uniform layer, which exhibits a highly oriented relationship to the Si in MS/SiNWs. However, annealing treatment may not necessarily lead to improvement of the quality of metal/Si layers. For example, in the high-temperature (900 °C) annealing of Co-implanted SiNWs, we observed that the number of $CoSi_2$ clusters decreased and some larger $CoSi_2$ particles formed with a size of a few times larger than that existed before annealing, as shown in Figure 4d. The results suggest that the small Co/Si clusters in close proximity interdiffused and aggregated to form larger particles during the annealing process. Such a phenomenon is known as Ostwald ripening or particle coarsening,[12] which largely reduces the total surface energy and therefore the system energy. The coarsening process may be enhanced by the nanosize effect. This is because the melting temperature (especially surface melting temperatures) of nanosize materials is generally reduced. The lower melting temperature would largely increase the surface diffusivity of atoms. A similar effect has been observed during annealing of SiNWs at high temperatures, where SiNWs may transform to nanoparticle chains so as to reduce surface energy.[13]

In summary, $NiSi_2$/Si and $CoSi_2$/Si have been synthesized on the surface of bare SiNWs using MEVVA ion source implantation. The SiO_x outer layer of the SiNWs was removed or reduced possibly due to sputtering during ion implantation. The formation of MS is expected to lead to improved electrical conductivity of SiNWs and provide selective electrical contacts to SiNWs. The structure of the MS/SiNWs layer is sensitive to annealing treatment. Under proper annealing conditions, the MS layer can exhibit a highly oriented relationship to the SiNW core.

[1] R. S. Wagner, W. C. Ellis, *Appl. Phys. Lett.* **1964**, *4*, 89.
[2] S. P. Murarka, *Metallization: Theory and Practice for VLSI and ULSI*, Butterworth-Heinemann, Woburn, MA **1993**.
[3] H. B. Ghozlene, P. Beaufrere, A. Authier, *J. Appl. Phys.* **1978**, *49*, 3998.
[4] H. Ishiwara, K. Hikosaka, S. Furukawa, *J. Appl. Phys.* **1978**, *50*, 5302.
[5] U. Koster, P. S. Ho, J. E. Lewis, *J. Appl. Phys.* **1978**, *53*, 7436.
[6] R. T. Tung, J. M. Poate, J. C. Bean, J. M. Gibson, D. C. Jacobson, *Thin Solid Films* **1982**, *93*, 77.
[7] A. E. White, K. T. Short, R. C. Dynes, J. P. Garno, J. M. Gibson, *Appl. Phys. Lett.* **1987**, *50*, 95.
[8] S. Mantl, *Mater. Sci. Rep.* **1992**, *8*, 1.
[9] I. G. Brown, J. E. Galvin, R. A. MacGrill, *Appl. Phys. Lett.* **1985**, *47*, 358.
[10] N. Wang, Y. H. Tang, Y. F. Zhang, C. S. Lee, S. T. Lee, *Chem. Phys. Lett.* **1999**, *299*, 237.
[11] S. T. Lee, Y. F. Zhang, N. Wang, Y. H. Tang, I. Bello, C. S. Lee, Y. W. Chung, *J. Mater. Res.* **1999**, *12*, 4503.
[12] W. Ostwald, *Z. Phys. Chem.* **1900**, *34*, 495.
[13] N. Wang, Y. H. Tang, Y. F. Zhang, C. S. Lee, S. T. Lee, *Phys. Rev. B* **1998**, *58*, R16 024.

Colloid Crystal Growth on Mesoscopically Patterned Surfaces: Effect of Confinement

By *Eugenia Kumacheva,* Robert Kori Golding, Mathieu Allard, and Edward H. Sargent*

Photonic crystals exhibit interesting physical phenomena[1] and enable novel optical devices.[2] The realization of photonic crystals based on ordering of monodispersed colloidal spheres followed by infiltration of high-refractive index materials possesses the appealing feature that large photonic crystals may be realized without recourse to top-down nanolithographic patterning.[3] However, existing approaches for organizing colloidal particles in ordered structures[4–10] provide no reproducible means of controlling the size and the

[*] Dr. E. Kumacheva, R. K. Golding
Department of Chemistry, University of Toronto
80 St. George Street, Toronto, Ontario, M5S 3H6 (Canada)
E-mail: ekumache@chem.utoronto.ca

M. Allard, Dr. E. H. Sargent
Department of Electrical and Computer Engineering
10 King's College, University of Toronto
Toronto, Ontario, M5S 3G4 (Canada)

density of defects that make up the resulting polycrystal. This militates against control over the establishment of delocalized Bloch waves inside the structures, just as amorphousness and polycrystallinity in electronic semiconductors impede the formation of sharply defined electronic bandgaps, electron wave coherence, and high-mobility electron transport. The reproducible realization of highly perfected single crystals is thus of critical importance in the practical exploitation of novel photonic crystal phenomena.

Recently, several experimental studies have demonstrated that confinement can significantly enhance colloid crystal growth and ultimately produce single-crystal or close-to-single crystal structure.[11] Here we show how transition from a disordered state to a strongly ordered state occurs in two-dimensional (2D) arrays of colloidal microspheres, following their confinement to progressively thinner gaps. The confinement induces disorder–order transition at a well-defined width of the gap, reminiscent of confinement-induced liquid-to-solid transition in simple liquids.[12,13]

We used electrodeposition of monodispersed charged colloidal spheres onto a substrate patterned with an array of electroconductive grooves whose progressively diminishing width was commensurate or incommensurate with the dimensions of a discrete number of colloidal spheres. In this approach, control over large-scale ordering did not rely on a submicrometer-scale surface template[14] but was achievable via a planar pattern whose scale was on the order of tens of micrometers, a regime readily accessed through coarse lithography, laser micromachining, and holography.

Here we focus on the results obtained for latex spheres of poly(methylmethacrylate) (PMMA) prepared by surfactant-free emulsion polymerization. The diameter of the particles was 0.58 μm, polydispersity index 1.03, and ξ-potential –54.9 mV at pH 5.46.

The surface patterning was realized by writing holographic gratings in thin negative photoresist layers (Shipley Microposit S1805), spin-coated on indium tin oxide (ITO) glass slides, using a helium–cadmium laser (35 mW beam at 442 nm). Exposure followed by development of the photoresist produced a pattern of periodically alternating isolating ribs and conductive grooves on the surface of ITO-covered slides (Fig. 1a). The width of the grooves, D, was varied from ca. 0.6 to 50 μm by changing the angle between the two interfering beams and the exposure time from 5 to 45 s. The height of the ribs was ca. 0.3 μm; smaller and larger heights were achievable through dilution of the photoresist solution and by using other photoresists (e.g., Shipley Microposit S1827), respectively. A typical topographic profile of the patterned surface is shown Figure 1b. The bottom of the conductive groove had a rms roughness not exceeding several nanometers, similar to the roughness of the surface of the uncoated ITO slides.

A schematic of the electrodeposition chamber is shown in Figure 1c. To avoid any effects associated with sedimentation of particles, electrophoresis was carried out against gravity. The speed of deposition, v, on the patterned anode was determined
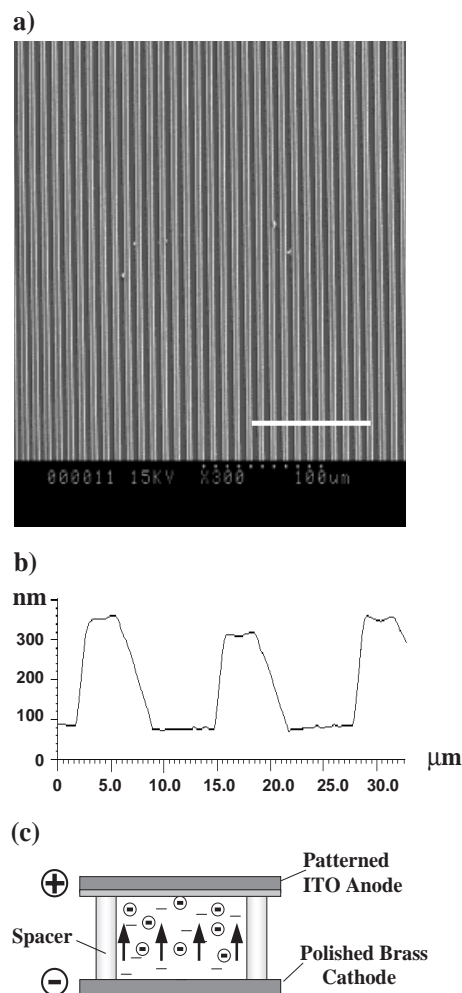

Fig. 1. a) SEM image of the patterned ITO surface. The scale bar is 100 μm. b) Typical atomic force microscopy (AFM) profile of the patterned ITO surface. The height of the isolating walls is ca. 300 nm. c) Schematic of the experimental setup used for anodic electrodeposition of the negatively charged PMMA particles. The electrodes are separated by a 5 mm spacer.

by the relation between the force imposed on particles by electric field and gravitational, Archimedes, and frictional forces as

$$v = \{uE - [d^2(\rho_p - \rho_w)g]\}/18\eta \tag{1}$$

where u is the electrophoretic mobility, E is the electric field, d is the diameter of the particles, ρ_p and ρ_w are the densities of PMMA spheres and water, respectively, g is the gravity acceleration, and η is the viscosity of the dispersion medium. The density of microsphere packing on the electrode and number of deposited layers were controlled by varying the time of deposition and the electric field strength. In a typical experiment, an electric field of 400 V/cm was applied for 90 s to the electrodes confining a 0.25 wt.-% dispersion of PMMA particles in a 50:50 mixture of ethanol and de-ionized water. Following electrodeposition, the samples were rinsed in deionized water and dried.

Figures 2a–c show typical scanning electron microscopy (SEM) images of the 2D microsphere arrays deposited on the non-patterned and patterned surfaces. No noticeable differ-
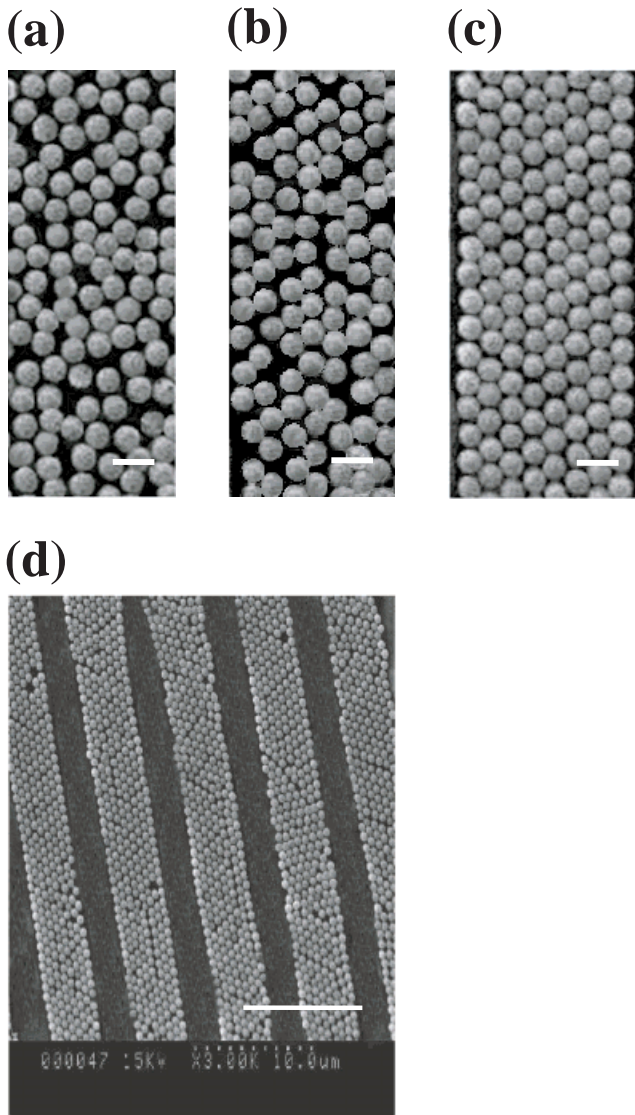
(a) (b) (c)

(d)

Fig. 2. SEM images of the colloidal arrays electrodeposited on non-patterned (a) and patterned (b–d) ITO surfaces. The widths of the grooves are 5.5 μm (b) and 4.2 μm (c,d). The SEM images of the colloidal arrays with the width 4.2 μm were cropped in (a) and (b). Scale bars are 1 μm (a–c) and 10 μm (d).

ence was observed in the structure of 2D colloidal arrays electrodeposited on non-patterned ITO surfaces and on the substrates patterned with conductive grooves whose width exceeded ca. 7.5 μm. The structure of the colloidal arrays was essentially disordered with occasional ordered domains not exceeding 20 μm^2 (Fig. 2a). Electrodeposition on the substrates patterned with grooves whose width was 6.0 ± 1.3 μm resulted in particle layering parallel to the rib walls, as is shown in Figure 2c. A dramatic enhancement in microsphere organization in 2D hexagonal close-packed arrays was observed for $D < 4.7$ μm, as is demonstrated in Figure 2c. The enhancing effect of confinement on colloid crystal growth was observed for the particles deposited into the grooves with the height of at least 0.3 μm and the width varying from 0.6 to 4.7 μm; the latter grooves confined nine layers of microspheres aligned parallel to the isolating ribs. Dilution of the

photoresist solution resulted in shallow grooves whose depth was not sufficient for enhanced ordering.

At the beginning of the electrodeposition process, the structure of the colloidal arrays in the grooves was essentially random, however, as more particles reached the electrode, microsphere reorganization in the grooves occurred by squeezing the newly arriving spheres between the already deposited particles and followed by synergistic particle rearrangement. This resulted in large-scale particle ordering, as is shown in Figure 2d for assembly of the colloidal spheres in 4.2 μm thick grooves.

Organization of particles in the grooves was governed by two processes: electrodeposition driven by particle coulombic interactions with the electrode surface[15] and in the later stage by electrohydrodynamic[4] and capillary forces. The role of electric field was dominant: in the control experiment casting of the PMMA dispersion on the patterned surfaces led to a very moderate ordering of the microspheres in the grooves with the area of ordered domains not exceeding ca. 30 μm.

A close inspection of particle arrays in the grooves with $D < 4.7$ μm revealed that microsphere organization was represented by two states: highly ordered hexagonal packing and random dense packing. As an example, Figures 3a–c show the
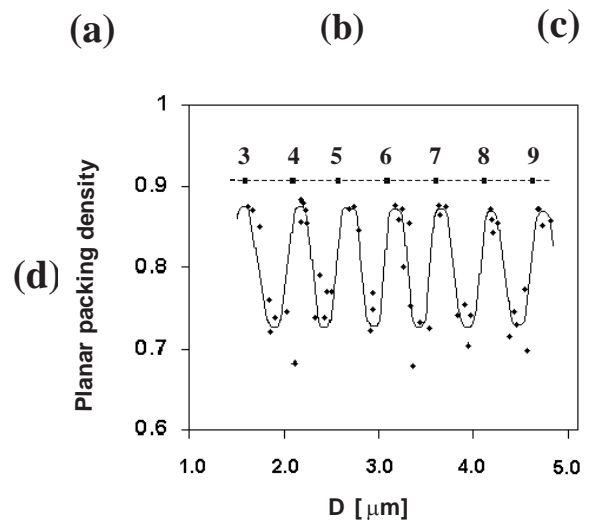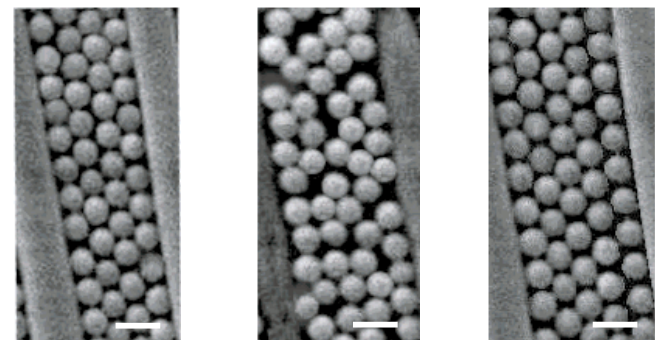

(a) (b) (c)

(d)

Fig. 3. Effect of confinement on organization of colloidal particles in the conductive groove. Order–disorder–order transition in colloidal arrays following progressive confinement of the colloid array. The width of the grooves in μm: 2.22 (a), 2.51 (b), 2.72 (c). d) Planar packing density profile $\phi = f(D)$ for the 2D array of colloidal microspheres. The dashed line shows the theoretical planar density of 0.9069 for a close-packed 2D hexagonal lattice.

SEM images of an order–disorder–order transition in particle arrays when D changed as $2.22 \rightarrow 2.51 \rightarrow 2.72$ μm, respectively. A quantitative measure of this effect was obtained by determining the planar packing density, ϕ[16] for the 2D arrays of particles in the grooves as a function of the groove width. In Figure 3d the graph $\phi = f(D)$ shows oscillations with the periodicity 0.52 ± 0.02 μm. Each maximum in ϕ of ca. 0.87 ± 0.02 corresponded to the high density hexagonal structure of the particle arrays containing a discrete number of layers aligned parallel to the wall. The values of ϕ for wells varied from ca. 0.67 to 0.81. Occasionally, square planar packing was observed with $\phi = 0.78$.

The maxima on the oscillating profile in Figure 2b were close to the 2D fractional density of 0.907 theoretically predicted for the six-fold geometry.[16] The theoretical width of the grooves, D_c, accommodating a discrete number of in-plane close-packed hexagonal particle layers were calculated as $D_c = 2R[(n-1)\cos30° + 1]$, where R is the radius of spheres and n is the number of layers of particles aligned parallel to the wall. The values of D_c were 5 ± 3 % smaller than the experimental values of groove widths providing strong microsphere ordering, a discrepancy presumably caused by a larger effective particle size due to electrostatic repulsion between the spheres. In contrast to this tolerable incommensurability, the defect disordered structure appeared from a strong mismatch between D_o and D exceeding 10–30 %. Similarly, no ordered structures could be obtained when the particle polydispersity exceeded 1.08 ± 0.02.

Confinement-induced ordering and oscillatory profile of particle planar packing density bear a striking resemblance to confinement-induced layering and solidification in thin layers of simple fluids with quasi-spherical molecules,[12,13] in which a) crystallization occurred when the width of the gap between the two confining walls became comparable with several molecular diameters and b) upon progressive thinning of the gap liquefaction of the solid-like lattice took place every time the thickness of the layer was not commensurate to the discrete number of the confined molecules.

Multilayer colloid crystal growth was achieved in a galvanostatic regime by increasing the time of electrodeposition from 90 s to ca. 2 min. In these experiments, the height of the rib of ca. 0.3 μm was insufficient in producing ordered arrays thicker than two particle layers. To provide out-of-plane ordering of up to five layers 2 μm high grooves were efficient.

The proposed approach has two important implications. First, it gives a new, very promising avenue for controlled growth of large-scale colloidal crystals. The speed of colloid crystal growth can be controlled via electrodeposition parameters such as voltage and time, and electrophoretic mobility of the particles, thus control over layer-by-layer deposition is possible. This feature makes it possible to examine defects emerging in the layers adjacent to the substrate. Moreover, in the second step electrodeposition of high-refractive index II–VI semiconductors in the interstitial spaces between the colloid spheres can be used for templating photonic crystals.[17] Second, this method shows a new way to study 2D and 3D confinement-induced order–disorder transitions in complex fluids.[18] Precise control of the degree of confinement is achieved by holographic patterning through the variation of widths of the grooves and heights of the ribs.

[1] S. John, *Phys. Rev. Lett.* **1987**, *58*, 2486.
[2] H. Kosaka, T. Kawashima, A. Tomita, M. Notomi, T. Tamamura, T. Sato, S. Kawakami, *Appl. Phys. Lett.* **1999**, *74*, 1370.
[3] a) A. Imhof, D. J. Pine, *Nature* **1997**, *389*, 948. b) B. T. Holland, C. F. Blanford, A. Stein, *Science* **1998**, *281*, 538. c) A. A. Zakhidov, R. H. Baughman, Z. Iqbal, C. X. Cui, I. Khayrullin, S. O. Dantas, J. Marti, V. G. Ralchenko, *Science* **1998**, *282*, 897. d) J. E. G. Wijnhoven, W. L. Vos, *Science* **1998**, *281*, 802.
[4] M. Trau, D. A. Saville, I. A. Aksay, *Science* **1996**, *272*, 706.
[5] a) H. Míguez, F. Meseguer, C. López, Á. Blanco, J. S. Moya, J. Requena, A. Mifsud, V. Fornés, *Adv. Mater.* **1998**, *10*, 480. b) K. E. Davis, W. B. Russel, W. J. Glantschnig, *J. Chem. Soc., Faraday Trans.* **1991**, *87*, 411.
[6] H. W. Deckman, J. H. Dunsmuir, *Appl. Phys. Lett.* **1982**, *41*, 377.
[7] N. D. Denkov, O. D. Velev, P. A. Kralchevsky, I. B. Ivanov, H. Yoshimura, K. Nagayama, *Nature* **1993**, *361*, 26.
[8] a) A. L. Rogach, N. A. Kotov, D. S. Koktysh, J. W. Ostrander, G. A. Ragoisha, *Chem. Mater.* **2000**, *12*, 2721. b) M. Holdado, F. Garsia-Santamaria, Á. Blanco, M. Ibisate, A. Cintas, H. Miguez, C. J. Serna, C. Molpceres, J. Requena, A. Mifsud, F. Meseguer, C. López, *Langmuir* **1999**, *15*, 4701. c) R. C. Hayward, D. A. Saville, I. A. Aksay, *Nature* **2000**, *404*, 56.
[9] O. Vickreva, O. Kalinina, E. Kumacheva, *Adv. Mater.* **2000**, *12*, 110.
[10] P. Jiang, J. F. Bertone, K. S. Hwang, V. L. Colvin, *Chem. Mater.* **1999**, *11*, 2132.
[11] a) E. Kim, Y. Jia, G. M. Whitesides. *Adv. Mater.* **1996**, *8*, 245. b) B. Gates, D. Qin, Y. Xia, *Adv. Mater.* **1999**, *11*, 466. c) K.-H. Lin, J. C. Crocker, V. Prasad, A. Schofield, D. A. Weitz, T. C. Lubensky, A. G. Yodh, *Phys. Rev. Lett.* **2000**, *85*, 1770. d) P. Yang, A. H. Rizvi, B. Messer, B. F. Chmelka, G. M. Whitesides, G. D. Stucky, *Adv. Mater.* **2001**, *13*, 427. e) G. A. Ozin, S. M. Yang, *Adv. Funct. Mater.* **2001**, *11*, 95.
[12] a) J. N. Israelachvili, P. M. McGuiggan, A. M. Homola, *Science* **1988**, *240*, 289. b) J. Van Alsten, S. Granick, *Phys. Rev. Lett.* **1988**, *61*, 2570. c) H. Yoshizawa, J. N. Israelachvili, *J. Chem. Phys.* **1993**, *75*, 140. d) J. Klein, E. Kumacheva, *Science* **1995**, *269*, 816.
[13] a) M. Schoen, D. J. Diestler, J. Cushman, *J. Chem. Phys.* **1987**, *87*, 5464. b) P. A. Thompson, M. O. Robbins, *Science* **1990**, *250*, 792. c) J. Gao, W. D. Luedtke, U. Landman, *Phys. Rev. Lett.* **1997**, *79*, 705. d) S. T. Cui, P. T. Cummings, H. D. Cochran, *J. Chem. Phys.* **2001**, *114*, 7189.
[14] A. V. Blaaderen, R. Ruel, P. Wiltzius, *Nature* **1997**, *385*, 321.
[15] In addition to Coulombic attraction, particle binding to the electrode was enhanced by the reaction of ionized surface carboxylic groups with H^+ ions produced by electrolysis of water on the anode. The latter mechanism led to adhesion of the particles to each other. When colloidal arrays were obtained by casting a latex dispersion on the patterned substrate, the sediment was easily removed from the surface by rinsing with water.
[16] R. M. German, *Sintering Theory and Practice*, Wiley, New York **1996**.
[17] P. V. Braun, P. Wiltzius, *Nature* **1999**, *402*, 603.
[18] A. P. Gast, W. B. Russel, *Phys. Today* **1998**, *51*, 24.